



**HAL**  
open science

## Effect of density step on stirring properties of a strain flow

M Gonzalez, P Paranthoën

► **To cite this version:**

M Gonzalez, P Paranthoën. Effect of density step on stirring properties of a strain flow. Fluid Dynamics Research, 2009, 41, pp.035508. 10.1088/0169-5983/41/3/035508 . hal-01415382

**HAL Id: hal-01415382**

**<https://hal.science/hal-01415382>**

Submitted on 13 Dec 2016

**HAL** is a multi-disciplinary open access archive for the deposit and dissemination of scientific research documents, whether they are published or not. The documents may come from teaching and research institutions in France or abroad, or from public or private research centers.

L'archive ouverte pluridisciplinaire **HAL**, est destinée au dépôt et à la diffusion de documents scientifiques de niveau recherche, publiés ou non, émanant des établissements d'enseignement et de recherche français ou étrangers, des laboratoires publics ou privés.

# Effect of density step on stirring properties of a strain flow

M. Gonzalez\* and P. Paranthoën

*CNRS, UMR 6614, Laboratoire de Thermodynamique, CORIA,*

*Site universitaire du Madrillet, 76801 Saint-Etienne du Rouvray, France*

---

## Abstract

The influence of steep density gradient upon stirring properties of a strain flow is addressed by considering the problem in which an interface separating two regions with different constant densities is stabilised within a stagnation-point flow. The existence of an analytic solution for the two-dimensional incompressible flow field allows the exact derivation of the velocity gradient tensor and of parameters describing the local flow topology. Stirring properties are affected not only through vorticity production and jump of strain intensity at the interface, but also through rotation of strain principal axes resulting from anisotropy of pressure Hessian. The strain persistence parameter, which measures the respective effects of strain and effective rotation (vorticity plus rotation rate of strain basis), reveals a complex structure. In particular, for large values of the density ratio it indicates dominating effective rotation in a restricted area past the interface. Information on flow structure derived from the Okubo-Weiss parameter, by contrast, is less detailed. The influence of the density step on stirring properties is assessed through the Lagrangian evolution of the gradient of a passive scalar. Even for a moderate density ratio, alignment of the scalar gradient and growth rate of its norm are deeply altered. Past the interface effective rotation indeed drives the scalar gradient to align

with a direction determined by the local strain persistence parameter, away from the compressional strain direction. The jump of strain intensity at the interface, however, opposes the lessening effect of the latter mechanism on the growth rate of the scalar gradient norm and promotes the rise of the gradient.

*Key words:* strain flow, density step, flow topology, stirring properties, passive scalar gradient

---

## 1 Introduction

In stratified environmental and engineering flows or in reacting flows where local heat release occurs velocity gradient properties are affected by spatial variations of density. Density gradients may thus indirectly play on stirring properties of flows through the local features of the velocity gradient. The influence of a density gradient upon velocity gradient properties has been tackled in some studies. In their classification of local flow topologies Chong *et al.* (1990) considered the case of compressible flows. Hua *et al.* (1998) have shown analytically how in geostrophic turbulence the topology of stirring undergoes the effect of a stable stratification through the velocity gradient. The interaction between strain, vorticity and density gradient in homogeneous sheared turbulence has been studied numerically by Diamessis and Nomura (2000). In combustion flows heat release may deeply influence mixing through scalar dissipation (Pantano *et al.* , 2003; Chakraborty and Swaminathan , 2007). This finding thus suggests a possible effect of density variations on the velocity gradient/scalar gradient interaction. In passing, it also questions the relevance to

---

\* Email address: Michel.Gonzalez@coria.fr

combustion of ‘cold-flow analyses’ of small-scale mixing. The small-scale structure of the velocity field in nonpremixed flames has been investigated in the numerical studies of Nomura and Elghobashi (1993) and Boratav *et al.* (1996, 1998). These authors showed how strain and vorticity properties – in particular, vorticity alignments – are changed by variable density via dilatational and baroclinic effects. Nomura and Elghobashi (1993) also studied the local flow topology using the classification of Chong *et al.* (1990) for compressible flows. Boratav *et al.* (1998) analysed the way in which buoyancy-influenced vorticity alignment indirectly affects the dissipation rate of fuel concentration. In addition, they examined how the properties of the pressure Hessian are changed by variable density. This is a key point, for the pressure Hessian contributes to the rotation of strain principal axes (Dresselhaus and Tabor , 1991; Nomura and Post , 1998; Lapeyre *et al.* , 1999) and may thus be indirectly involved in the small-scale mixing process through alignment mechanisms.

The present study is specially focused on the effect of local steep density gradients. The latter are produced, for instance, in reacting flows with significant heat release. For the purpose of our analysis we consider the flow field of a model problem taken from flame studies in which an interface stabilised in a pure straining velocity field divides the flow in two regions with different densities. The two dimensional inviscid problem in which each flow region is assumed to be incompressible has an analytic solution (Kim and Matalon , 1988). The main advantage of the approach lies in that the flow field is completely known and its properties in terms of strain, vorticity, pressure Hessian ... can therefore be derived exactly. In particular, parameters relevant to local flow topology and stirring properties such as the Okubo-Weiss parameter or the strain persistence parameter can be expressed analytically. This makes

it possible to examine thoroughly the way in which they are influenced by the density step. Finally, the strain persistence parameter is used to track the Lagrangian evolution of the gradient of a passive scalar in terms of orientation and norm growth rate. The effects of the density step upon the stirring mechanism, then, are precisely revealed.

The problem under study and the relating flow field are described in Section 2. The flow structure derived from the velocity gradient tensor is studied in Section 3. In particular, the way in which the level of the density step affects the local flow topology is closely analysed through the behaviour of the strain persistence parameter. In Section 4 we show how the local alignment and growth rate of the gradient of a passive scalar and thus stirring properties are influenced by the density step. Conclusions are drawn in Section 5

## **2 Flow conditions and dynamic field equations**

We consider the stationary problem analysed by Kim and Matalon (1988) which consists of a plane premixed flame stabilised in the stagnation-point flow of a body (Fig. 1). The flame thickness is assumed to be much smaller than its standoff distance. At the flow scale, the flame front may thus be regarded as a discontinuity separating unburnt from lighter burnt gases. In addition, the flow is considered to be inviscid and the flowfield in each region of constant density ( $\rho_u$  and  $\rho_b$ , respectively, in the unburnt and burnt gases) is described by the two-dimensional incompressible Euler equations. Stability analysis has been made by Kim and Matalon (1990) and Jackson and Matalon (1993). In the present study stability is ensured according to the criteria derived by Kim and Matalon (1990) for the two-dimensional case, in particular, unity Lewis

number is prescribed.

The equations are made dimensionless by using the adiabatic flame speed and the length scale characterising the standoff distance as velocity and length units; density, temperature and pressure are normalised by their respective values in the unburnt gas. Kim and Matalon (1988) derived the velocity field from Euler and continuity equations combined with Rankine-Hugoniot relations for the jumps at the interface and boundary conditions for velocity upstream ( $x \rightarrow \infty$ ) and at the surface of the body ( $x = 0$ ). The flame is found to stabilise at distance  $d$  from the body which, for unity Lewis number and plane geometry, is given by:

$$d = \frac{2\gamma \arctan [(\gamma - 1)^{1/2}]}{\sigma_0(\gamma - 1)^{1/2}}. \quad (1)$$

In the case of non-unity Lewis number,  $d$  is given by a transcendental equation which precludes a complete analytic study. Parameters  $\gamma = \rho_u/\rho_b$  and  $\sigma_0$  are, respectively, the thermal expansion coefficient (or density ratio) and the intensity of the imposed strain. Strain intensity is defined as  $\sigma = (\sigma_n^2 + \sigma_s^2)^{1/2}$  where  $\sigma_n = \partial u/\partial x - \partial v/\partial y$  and  $\sigma_s = \partial v/\partial x + \partial u/\partial y$  are the normal and shear components of strain. In the unburnt region  $\sigma = \sigma_0$ . The coordinate system is defined in Fig. 1 and  $u$  and  $v$  are the velocity components normal and parallel to the interface, respectively.

The velocity and pressure fields are described by the following equations (Kim and Matalon, 1988).

For  $x > d$ :

$$\rho = 1, \quad (2)$$

$$u = -\frac{1}{2}\sigma_0(x - a), \quad (3)$$

$$v = \frac{1}{2}\sigma_0 y, \quad (4)$$

$$p = p_a - \frac{1}{8}\sigma_0^2 [(x - a)^2 + y^2], \quad (5)$$

where  $p_a$  is the pressure at the virtual stagnation point,  $(x, y) = (a, 0)$ , and constant  $a$  is given by:

$$a = \left[ 1 - \frac{(\gamma - 1)^{1/2}}{\gamma \arctan [(\gamma - 1)^{1/2}]} \right] d. \quad (6)$$

For  $x < d$ :

$$\rho = \frac{1}{\gamma}, \quad (7)$$

$$u = -\frac{1}{2}\sigma_0 \delta \sin(kx), \quad (8)$$

$$v = \frac{1}{2}\sigma_0 k \delta y \cos(kx), \quad (9)$$

$$p = p_s - \frac{1}{8}\sigma_0^2 \left[ \frac{\delta^2}{\gamma} \sin^2(kx) + y^2 \right], \quad (10)$$

with pressure at the actual stagnation point,  $p_s$ , given by:

$$p_s = p_a - \frac{1}{8}(\gamma - 1)(d - a)^2 \sigma_0^2, \quad (11)$$

and constants  $\delta$  and  $k$  by:

$$\delta = \gamma \left( \frac{\gamma}{\gamma - 1} \right)^{1/2} (d - a), \quad (12)$$

and

$$k = \frac{(\gamma - 1)^{1/2}}{\gamma(d - a)}. \quad (13)$$

The dynamic field is completely defined by (1) to (13) and parameters  $\gamma$  and  $\sigma_0$ . Note that from (1) and (6)  $d - a$  only depends on the imposed strain as  $d - a = 2/\sigma_0$ . In the following we use the above model for deriving the change in flow structure brought about by the density step. We are more specifically

interested in stirring properties resulting from the flow topology determined by the velocity gradient tensor.

### 3 Influence of the density step on flow structure

The velocity gradient tensor can be derived analytically from (1) – (13). In particular, calculation of its symmetric and antisymmetric parts, namely strain and rotation is straightforward.

The properties of the prescribed strain flow ( $x > d$ ) are obviously those of a pure straining motion with  $\sigma_n = -\sigma_0$  and  $\sigma_s = 0$ ; the Okubo-Weiss parameter,  $Q = \sigma^2 - \omega^2$ , where  $\omega = \partial v/\partial x - \partial u/\partial y$  is the vorticity, amounts to  $Q = \sigma_0^2$ . The pressure Hessian,  $\mathbf{H}$ , is isotropic; from (5):

$$H_{ij} = \frac{1}{\rho} \frac{\partial^2 p}{\partial x_i \partial x_j} = -\frac{1}{4} \sigma_0^2 \delta_{ij}. \quad (14)$$

The strain persistence parameter,  $r$ , is defined as (Lapeyre *et al.*, 1999):

$$r = \frac{\omega + \Omega}{\sigma}, \quad (15)$$

where  $\Omega$  is the rotation rate of strain principal axes (Lapeyre *et al.*, 1999):

$$\Omega = \frac{1}{\sigma^2} \left[ \sigma_s \left( \frac{d\sigma_n}{dt} \right) - \sigma_n \left( \frac{d\sigma_s}{dt} \right) \right]. \quad (16)$$

Because it includes the acceleration gradient tensor via the strain derivatives, the strain persistence parameter is more general than the Okubo-Weiss parameter. In particular, accounting for the Lagrangian variation of strain allows a better estimate of stirring properties (Hua and Klein, 1998; Lapeyre *et al.*, 1999). Dominating strain corresponds to  $r^2 < 1$ , while effective rotation prevails if  $r^2 > 1$  and balance occurs for  $r^2 = 1$ . Analysis of stirring through the

behaviour of a passive scalar gradient in terms of orientation and norm based on the latter different regimes has been performed by Lapeyre *et al.* (1999). They assumed  $r$  varying “slowly” along the Lagrangian trajectories, that is, on a time scale much larger than the gradient response time scale. The effect of fluctuations of  $r$  faster than the response of the scalar gradient has been studied by Garcia *et al.* (2005, 2008). In an inviscid incompressible flow equations for  $\sigma_n$  and  $\sigma_s$  only include the pressure Hessian components (Lapeyre *et al.*, 1999):

$$\frac{d\sigma_n}{dt} = \frac{1}{\rho} \frac{\partial^2 p}{\partial y^2} - \frac{1}{\rho} \frac{\partial^2 p}{\partial x^2}, \quad (17)$$

$$\frac{d\sigma_s}{dt} = -\frac{2}{\rho} \frac{\partial^2 p}{\partial x \partial y}, \quad (18)$$

and reveal that the rotation rate of strain axes,  $\Omega$ , results from the anisotropic part of  $\mathbf{H}$ . Equations (14) and (16) to (18) thus show that in the imposed straining flow  $\Omega = 0$  and, as a consequence,  $r = 0$  which indicates perfectly persistent strain. The Okubo-Weiss and strain persistence parameters obviously agree in this simple case. However, depending on the density ratio, they may differ from one another in their diagnoses in the flow region past the interface as shown in the following.

Beyond the interface ( $x < d$ ) the velocity gradient has a rotational part due to vorticity production at the discontinuity. Strain and vorticity are derived from (8), (9), (12) and (13):

$$\sigma_n = -\sigma_0 \gamma^{1/2} \cos(kx), \quad (19)$$

$$\sigma_s = -\frac{1}{2} \sigma_0 \gamma^{1/2} ky \sin(kx), \quad (20)$$

$$\omega = -\frac{1}{2} \sigma_0 \gamma^{1/2} ky \sin(kx). \quad (21)$$

At the interface, the normal component of strain is conserved,  $\sigma_n(d^-) = \sigma_n(d^+) = -\sigma_0$ , while the shear component undergoes a step from  $\sigma_s(d^+) = 0$

to  $\sigma_s(d^-) = -\sigma_0(\gamma - 1)^{1/2} \arctan [(\gamma - 1)^{1/2}] y/2d$  resulting in a step in strain intensity expressed by:

$$\sigma(d^-) = \sigma(d^+) \left[ 1 + (\gamma - 1) \arctan^2 [(\gamma - 1)^{1/2}] \frac{y^2}{4d^2} \right]^{1/2} \quad (22)$$

The Okubo-Weiss parameter depends on both imposed strain and density ratio and varies with  $x$  as:

$$Q = \sigma_0^2 \gamma \cos^2(kx).$$

Because from (1) and (13)  $kx \leq kd = \arctan [(\gamma - 1)^{1/2}] < \pi/2$ , parameter  $Q$  never takes a zero value. It grows with increasing density ratio and is strictly positive thus indicating prevailing strain.

The pressure Hessian derived from (7) and (10) (using also (12) and (13)) is anisotropic:

$$\frac{1}{\rho} \frac{\partial^2 p}{\partial x^2} = -\frac{1}{4} \sigma_0^2 \gamma \cos(2kx), \quad (23)$$

$$\frac{1}{\rho} \frac{\partial^2 p}{\partial y^2} = -\frac{1}{4} \sigma_0^2 \gamma, \quad (24)$$

$$\frac{1}{\rho} \frac{\partial^2 p}{\partial x \partial y} = \frac{1}{\rho} \frac{\partial^2 p}{\partial y \partial x} = 0. \quad (25)$$

From (13) and (23) it is clear that anisotropy is caused by the density step in  $x$  direction (which was foreseeable) and that isotropy of the pressure Hessian is retrieved for  $\gamma = 1$ . The level of anisotropy of  $\mathbf{H}$  is given by the anisotropy tensor,  $\mathbf{A}$ , defined by:

$$A_{ij} = \frac{2H_{ij} - H_{\alpha\alpha} \delta_{ij}}{H_{\alpha\alpha}}. \quad (26)$$

From (23) – (26):

$$A_{11} = -A_{22} = -\tan^2(kx),$$

and

$$A_{12} = A_{21} = 0.$$

The norm of tensor  $\mathbf{A}$ ,  $|\mathbf{A}| = \sqrt{2} \tan^2(kx)$ , is plotted in Fig. 2 for different values of  $\gamma$ . As  $\gamma$  is increased, the level of anisotropy grows and the largest anisotropy is restricted to a region closer to the interface. Defining  $x_{1/2}^*$  as the location in  $x/d$  where  $|\mathbf{A}|$  reaches half its maximum value, it is straightforward to show that

$$x_{1/2}^* = \frac{\arctan \left[ \left( \frac{\gamma-1}{2} \right)^{1/2} \right]}{\arctan \left[ (\gamma-1)^{1/2} \right]},$$

and, then,  $x_{1/2}^*$  tends to unity with increasing  $\gamma$ . Note that plotting results (possibly normalised by the imposed strain,  $\sigma_0$ , when needed) in function of  $x/d$ ,  $y/d$  or  $\sigma_0 t$  (for Lagrangian tracking) allows to get rid of explicit dependence on  $\sigma_0$  and to restrict the analysis to the effects of density ratio.

The anisotropy of the pressure Hessian results in rotation of the strain principal axes. Using (16) with (17) – (20) and the components of the pressure Hessian given by (23) – (25):

$$\Omega = \frac{\sigma_0 \gamma^{1/2} k y \sin(kx) \tan^2(kx)}{4 + k^2 y^2 \tan^2(kx)}. \quad (27)$$

It is worth noticing that from their respective signs the rotation rate of strain basis,  $\Omega$  and vorticity,  $\omega$  (given by (21)), oppose each other.

The strain persistence parameter, then, is derived from (15) together with (19) – (21) and (27):

$$r = - \frac{[4 + (k^2 y^2 - 2) \tan^2(kx)] k y \tan(kx)}{[4 + k^2 y^2 \tan^2(kx)]^{3/2}}.$$

Function  $r$  depends on density ratio through  $k$  given by (13). It is antisymmetric in  $y$  and tends to -1 from above as  $y$  tends toward  $+\infty$  and to 1 from below as  $y$  tends toward  $-\infty$ . A closer analytic examination reveals a rather rich behaviour that depends on the value of the density ratio. For  $\gamma \leq 3$ ,  $r$  is a monotonous decreasing function as shown in Fig. 3. For  $3 < \gamma \leq 9$ , extrema

appear near the interface, in a region defined by  $(x/d)_1 < x/d \leq 1$  (Fig. 4). Finally, if  $\gamma > 9$ ,  $r$  has a three-layered structure in  $x$ ;  $x/d \leq (x/d)_1$ :  $r$  is monotonous and decreasing;  $(x/d)_1 < x/d \leq (x/d)_2$ :  $r$  has extrema within the bounds -1 and 1;  $(x/d)_2 < x/d$ : the extrema exceed -1 and 1. This behaviour is displayed in Fig. 5. The threshold values  $(x/d)_1$  and  $(x/d)_2$  are given by:

$$\left(\frac{x}{d}\right)_1 = \frac{\arctan \sqrt{2}}{\arctan [(\gamma - 1)^{1/2}]},$$

and

$$\left(\frac{x}{d}\right)_2 = \frac{\arctan(2\sqrt{2})}{\arctan [(\gamma - 1)^{1/2}]},$$

and, as  $\gamma$  is increased, tend to constant values, namely  $(2 \arctan \sqrt{2})/\pi \simeq 0.608$  and  $[2 \arctan(2\sqrt{2})]/\pi \simeq 0.784$ . Figure 6 shows the two-dimensional field of  $r^2$  derived for a large value of the density ratio,  $\gamma = 10$ . Beyond the interface strain significantly dominates only in the vicinity of the plane of symmetry and of the slip boundary located at  $x/d = 0$ .

The evolution of  $r$  at large density ratio is explained by the rotation of strain principal axes. The vorticity-to-strain ratio defined as  $R = \omega/\sigma$  discarding the rotation rate of strain basis,  $\Omega$ , has a simpler behaviour. From (19) – (21):

$$R = -\frac{ky \tan(kx)}{[4 + k^2y^2 \tan^2(kx)]^{1/2}},$$

which shows that  $R$  is monotonous and bounded by -1 and 1 no matter the value of the density ratio. This is in no way surprising, for the criterion based on  $R$  only includes vorticity and strain and therefore amounts to the Okubo-Weiss criterion. Figures 7 and 8 display profiles of  $R$  for  $\gamma = 2$  and  $\gamma = 10$ , respectively. Better still, from (15) and the fact that from (21) and (27)  $\omega$  and  $\Omega$  have opposed signs,  $r$  starts developing a positive (resp. negative) extremum for  $y > 0$  (resp.  $y < 0$ ), near the origin, provided that  $|\Omega/\omega| > 1$ . From the

exact expression for  $\Omega/\omega$  derived using (21) and (27), it can be checked that  $|\Omega/\omega| > 1$  for  $\gamma > 3$ . The region where  $|\Omega/\omega| > 1$  is found to coincide with the one where  $r$  displays extrema. It is also found that in the present case  $|r| > 1$  for  $|\Omega/\omega| > 4$ .

Since in the problem under study the solution given by (3) – (6) and (8) – (13) depends on Lewis number through distance  $d$  (Kim and Matalon , 1988), the above threshold values for  $\gamma$  and  $x/d$  derived in the case of unity Lewis number are not universal. Nevertheless, the analysis leads to the conclusion that past the density interface parameter  $r$  indicates dominating strain except when the density ratio is large enough; in this case, effective rotation prevails near the plane of symmetry, in a region close to the interface.

#### 4 Consequences for alignment and stirring properties

Stirring and mixing properties of a flow field can be analysed through the evolution of the gradient of an advected passive scalar. In this view alignment of the scalar gradient with respect to the local strain principal axes is a key mechanism (Pumir , 1994; Vedula *et al.* , 2001; Brethouwer *et al.* , 2003). The increase of the gradient norm brought about by alignment with the local compressional direction causes enhancement of mixing through acceleration of molecular diffusion.

Lapeyre *et al.* (1999) have shown that in two-dimensional flows the opposed effects of strain and effective rotation result in the existence of directions that are mostly different from those of strain principal axes. Their analysis is based on the equation in the strain basis for the orientation of the gradient of a non-

diffusive passive scalar:

$$\frac{d\zeta}{d\tau} = r - \cos \zeta. \quad (28)$$

In the fixed frame of reference the scalar gradient is defined by vector  $\mathbf{G} = |\mathbf{G}|(\cos \theta, \sin \theta)$  with  $\zeta = 2(\theta + \Phi)$  and  $\Phi$  gives the orientation of the strain principal axes through  $\tan(2\Phi) = \sigma_n/\sigma_s$ . Note that the rotation rate,  $\Omega$ , of the strain principal axes defined by (16) coincides with  $2d\Phi/dt$ . Time  $\tau$  is a strain normalised time:

$$\tau = \int_0^t \sigma(t') dt',$$

where  $t$  stands for the Lagrangian time and  $\sigma$  for strain intensity. Assuming slow variations of  $r$  along Lagrangian trajectories, Lapeyre *et al.* (1999) showed how the local flow topology determines the orientation of the scalar gradient. If strain prevails over effective rotation ( $r^2 < 1$ ), the orientation equation (28) has a stable fixed point,

$$\zeta_{eq}(r) = -\arccos r, \quad (29)$$

corresponding to an equilibrium orientation. It is only in the special case  $r = 0$  – i.e. in the pure hyperbolic regime – that the equilibrium orientation,  $\zeta_{eq}$ , coincides with the local compressional direction,  $\zeta_c = -\pi/2$ , which corresponds to  $\theta = -\Phi - \pi/4$  in the fixed frame of reference. When strain and effective rotation balance each other ( $r^2 = 1$ ), the equilibrium orientation is a bisector of strain principal axes. If effective rotation dominates ( $r^2 > 1$ ), the scalar has no equilibrium orientation, but a most probable one coinciding with a bisector of the strain basis. From the numerical simulations of Lapeyre *et al.* (1999) in two-dimensional turbulence it appears that in strain-dominated regions the scalar gradient statistically aligns better with the local equilibrium orientation than with the compressional direction. In fact, Garcia *et al.* (2005, 2008) have shown that the scalar gradient aligns with the equilibrium direc-

tion rather than with the compressional one provided that its response time scale to  $r$  fluctuations is short enough compared to the Lagrangian time scale of  $r$ .

In the above approach the equation for the norm of the scalar gradient is (Lapeyre *et al.*, 1999):

$$\frac{2}{|\mathbf{G}|} \frac{d|\mathbf{G}|}{dt} = -\sigma \sin \zeta,$$

and obviously defines the local growth rate of the gradient norm as  $-\sigma \sin \zeta$ . Clearly, alignment with the compressional direction,  $\zeta = \zeta_c = -\pi/2$ , corresponds to the maximum growth rate. The growth rate in the unaltered region,  $x > d$ , obviously amounts to  $\sigma_0$ .

The local stirring properties of the flow under study can be derived from the field of the strain persistence parameter,  $r$ . In particular, the local equilibrium orientation is known through (29). Figure 9 displays the field of variable  $\Delta\zeta = |2[\zeta_{eq}(r) + \pi/2]/\pi|$  in the case of density ratio  $\gamma = 6$ . For the latter value of  $\gamma$  the whole flow is dominated by strain and  $\zeta_{eq}$  is defined everywhere. Variable  $\Delta\zeta$  ranges from 0 to 1 and gives the normalised difference between the local equilibrium and compressional directions. It takes the maximum value,  $\Delta\zeta = 1$ , for  $\zeta_{eq}$  corresponding to a bisector of the strain principal axes, namely  $\zeta_{eq} = 0$  or  $\zeta_{eq} = -\pi$  which coincide, respectively, with directions  $-\Phi$  and  $-\Phi - \pi/2$  in the fixed frame of reference. From Fig. 9 it is clear that past the interface  $\zeta_{eq}$  significantly departs from  $\zeta_c$  over most of the flow field except near the plane of symmetry and the slip boundary where strain significantly prevails over effective rotation. For  $x/d > 1$  pure strain makes the equilibrium orientation coincide with the compressional direction. According to the analysis of function  $r$  we made in Section 3, the difference  $\Delta\zeta$  obviously

tends to its maximum value with increasing  $y/d$ .

The limitation of stirring properties which would result from alignment with the local equilibrium orientation instead of the compressional direction is given by the theoretical growth rate, normalised by local strain,  $\eta_{eq}/\sigma = -\sin[\zeta_{eq}(r)] = \eta_{eq}^*$  (Fig. 10). As expected,  $\eta_{eq}^*$  is close to its maximum value near the plane of symmetry and the slip boundary where the equilibrium and compressional directions almost coincide. However,  $\eta_{eq}^*$  displays lower values over the rest of the flow field and even tends to 0 for large values of  $y/d$ . This trend results from  $\zeta_{eq}$  drawing near values 0 or  $-\pi$  as  $r$  tends toward 1 or -1, respectively. But the step in strain intensity given by (22) overcomes the effect of possible misalignment of the scalar gradient with respect to the compressional direction. Figure 11 shows the field of theoretical growth rate normalised by the imposed strain,  $\eta_{eq}/\sigma_0 = \sigma \sin[\zeta_{eq}(r)]/\sigma_0$ , and reveals the gain in growth rate at the interface caused by the step in strain intensity.

The response of a passive scalar gradient to the variations of strain persistence along Lagrangian trajectories brings further information. Equation (28) has been solved starting from initial conditions at the interface ( $x/d = 1$ ) for different values of  $y/d$ , namely  $y(0)/d = 1, 2, 5$  and 10 and density ratio  $\gamma = 6$ . Figure 12 shows the corresponding trajectories (cut at  $y/d = 100$ ). Initial conditions for velocity are given by (8) and (9) with  $x = d$ . Initially, the value of strain intensity is the imposed strain,  $\sigma_0$ , strain persistence,  $r$ , is zero and scalar gradient orientation is  $\zeta = \zeta_c = -\pi/2$ .

Figure 13 displays the trend of strain persistence toward its zero, pure hyperbolic value after the sharp change at the interface. The larger  $y(0)/d$ , the deeper the variation caused by the interface and the slower the evolution of

$r$ ; at  $\sigma_0 t = 100$   $|r|$  is close to 0.1 if  $y(0)/d = 1$ , but is around 0.7 in the case  $y(0)/d = 10$ . As expected, the local equilibrium orientation displays a similar behaviour (Fig. 14): for  $y(0)/d = 1$   $\zeta_{eq}$  almost retrieves its initial value,  $\zeta_c$ , at  $\sigma_0 t = 100$ ; for  $y(0)/d = 10$   $\zeta_c - \zeta_{eq}$  is still greater than  $0.2\pi$ . Now, the local, instantaneous orientation of the scalar gradient coincides with  $\zeta_{eq}$  only if its response time scale is short enough as compared to the time scale of  $r$  variations (Garcia *et al.*, 2005, 2008). Figure 15 shows that after  $\sigma_0 t = 2$  this condition is realized and  $\zeta$  varies as  $\zeta_{eq}$  no matter the value of  $y(0)/d$ . The actual growth rate of the scalar gradient norm thus coincides with the theoretical growth rate (Fig. 11) over most of the field past the interface and, as shown in Fig. 16, reveals a significant change of stirring properties with increasing  $y(0)/d$ . For long times,  $\zeta$  tends to  $\zeta_{eq} = -\arccos r$ , with  $r$  tending to 0; in addition, from (19) and (20) strain intensity,  $\sigma$ , tends to  $\gamma^{1/2}\sigma_0$  with  $x$  tending to 0. This makes the actual normalised growth rate,  $\eta/\sigma_0 = -\sigma \sin \zeta/\sigma_0$ , tends to  $\gamma^{1/2}$ . At the interface,  $\zeta$  is close to  $\zeta_c$  and the jump of  $\eta/\sigma_0$  coincides with the jump of strain intensity given by (22) and is of the order of  $(\gamma - 1)^{1/2} \arctan [(\gamma - 1)^{1/2}] y/2d$ .

## 5 Conclusion

The flow field resulting from stabilisation of an infinitely thin flame within a stagnation-point flow has been used for studying analytically the effect of a density step upon the structure and stirring properties of a straining flow. The analysis rests on the velocity gradient tensor and subsequent parameters indicating the local flow topology.

In addition to vorticity production and rise of strain intensity, the density

step causes rotation of strain principal axes through anisotropy of the pressure Hessian. Strain basis rotation and vorticity – the sum of which corresponds to effective rotation – do not combine, but oppose each other. The Okubo-Weiss parameter, which is only based on strain and vorticity, is sensitive to the density step and indicates prevailing strain whatever the value of the density ratio. Because it accounts for the acceleration gradient through the rotation rate of the strain basis, the strain persistence parameter betrays a more subtle behaviour. More specifically, it reveals the existence of a restricted area past the interface where strain is reduced relatively to effective rotation as density ratio is increased. For large values of the density ratio, strain basis rotation overcomes vorticity and effective rotation prevails over strain in this region of the flow.

Moreover, alignment properties of the gradient of a passive scalar and relating stirring properties of the flow field can be derived from the strain persistence parameter. For a moderate value of the density ratio, the difference between the equilibrium orientation of the scalar gradient resulting from the opposed effects of strain and effective rotation and the compressional direction is significant over most of the flow field beyond the interface. This misalignment with respect to compressional direction tends to lessen the growth rate of the gradient norm, but is overcome by the rise of strain intensity. Lagrangian analysis shows that past the interface the local, instantaneous orientation of the gradient of a passive scalar rapidly coincides with the equilibrium orientation and confirms the change in gradient growth rate (hence in stirring properties) brought about by the density step.

In this two-dimensional inviscid flow rotation of the strain principal axes is only caused by anisotropy of the pressure Hessian, while in the three-

dimensional case it also results from local vorticity. It would therefore be worth defining a three-dimensional flow in which the question could be re-examined. The strain/vorticity interaction also makes the three-dimensional case more complex. Another extension of the work should consist in relaxing the assumption of an infinitely thin density interface by defining a finite length scale of the density gradient. The analytic approach would certainly be harder, but numerical computation could be used for this purpose.

## References

- Boratav, O. N., Elghobashi, S. E. and Zhong, R. 1996. On the alignment of the  $\alpha$ -strain and vorticity in turbulent nonpremixed flames. *Phys. Fluids* **8**, 2251-2253.
- Boratav, O. N., Elghobashi, S. E. and Zhong, R. 1998. On the alignment of strain, vorticity and scalar gradient in turbulent, buoyant, nonpremixed flames. *Phys. Fluids* **10**, 2260-2267.
- Brethouwer, G., Hunt, J. C. R. and Nieuwstadt, F. T. M. 2003. Micro-structure and Lagrangian statistics of the scalar field with a mean gradient in isotropic turbulence. *J. Fluid Mech.* **474**, 193–225.
- Chakraborty, N. and Swaminathan, N. 2007. Influence of the Damköhler number on turbulence-scalar interaction in premixed flames. I. Physical insight. *Phys. Fluids* **19**, 045103.
- Chong, M. S., Perry, A. E. and Cantwell, B. J. 1990. A general classification of three-dimensional flow fields. *Phys. Fluids* **2**, 765–777.
- Diamessis, P. J. and Nomura, K. K. 2000. Interaction of vorticity, rate-of-strain and scalar gradient in stratified homogeneous sheared turbulence *Phys. Fluids* **12**, 1166–1188.

- Dresselhaus, E. and Tabor, M. 1991. The kinematics of stretching and alignments of material elements in general flow fields. *J. Fluid Mech.* **236**, 415–444.
- Garcia, A., Gonzalez, M. and Paranthoën P. 2005. On the alignment dynamics of a passive scalar gradient in a two-dimensional flow. *Phys. Fluids* **17**, 117102.
- Garcia, A., Gonzalez, M. and Paranthoën P. 2008. Nonstationary aspects of passive scalar gradient behaviour. *Eur. J. Mech. Fluids B/Fluids* **27**, 433–443.
- Hua, B. L. and Klein, P. 1998. An exact criterion for the stirring properties of nearly two-dimensional turbulence. *Physica D* **113**, 98–110.
- Hua, B. L., McWilliams, J. C. and Klein, P. 1998. Lagrangian acceleration in geostrophic turbulence. *J. Fluid Mech.* **366**, 87–108.
- Jackson, T. L. and Matalon, M. 1993. Stability of a premixed flame in stagnation point flow against general disturbances. *Combust. Sci. Tech.* **90**, 385–403.
- Kim, Y. D. and Matalon, M. 1988. Propagation and extinction of a flame in a stagnation-point flow. *Combust. Flame* **73**, 303–313.
- Kim, Y. D. and Matalon, M. 1990. On the stability of near-equidiffusional strained premixed flames. *Combust. Sci. Tech.* **69**, 85–97.
- Lapeyre, G., Klein, P. and Hua B. L. 1999. Does the tracer gradient vector align with the strain eigenvector in 2D turbulence? *Phys. Fluids* **11**, 3729–3737.
- Nomura, K. K. and Elghobashi, S. E. 1993. The structure of inhomogeneous turbulence in variable density nonpremixed flames. *Theoret. Comput. Fluid Dynamics* **5**, 153–175.
- Nomura, K. K. and Post, G. K. 1998. The structure and dynamics of vorticity

- and rate of strain in incompressible homogeneous turbulence. *J. Fluid Mech.* **377**, 65–97.
- Pantano, C., Sarkar, S. and Williams, F. A. 2003. Mixing of a conserved scalar in a turbulent reaction shear layer. *J. Fluid Mech.* **481**, 291–328.
- Pumir, A. A numerical study of the mixing of a passive scalar in three dimensions in the presence of a mean gradient. *Phys. Fluids* **6**, 2118–2132.
- Vedula, P., Yeung, P. K. and Fox, R. O. 2001. Dynamics of scalar dissipation in isotropic turbulence: a numerical and modelling study. *J. Fluid Mech.* **554**, 457–475.

## FIGURE CAPTION

FIGURE 1. Stagnation-point flow altered by the density step. Streamlines are plotted for density ratio  $\gamma = 6$ .

FIGURE 2. Effect of density ratio on the norm of the anisotropy tensor of pressure Hessian.

FIGURE 3. Profiles of strain persistence parameter for density ratio  $\gamma = 2$ . Solid:  $x/d = 0.25$ ; dashed:  $x/d = 0.50$ ; dashdot:  $x/d = 0.75$ ; dotted:  $x/d = 1.0$ .

FIGURE 4. Profiles of strain persistence parameter for density ratio  $\gamma = 6$ . Solid:  $x/d = 0.25$ ; dashed:  $x/d = 0.50$ ; dashdot:  $x/d = 0.75$ ; dotted:  $x/d = 0.90$ ; longdash:  $x/d = 1.0$ .

FIGURE 5. Profiles of strain persistence parameter for density ratio  $\gamma = 10$ . Solid:  $x/d = 0.25$ ; dashed:  $x/d = 0.50$ ; dashdot:  $x/d = 0.75$ ; dotted:  $x/d = 0.90$ ; longdash:  $x/d = 1.0$ .

FIGURE 6. Field of strain persistence parameter – squared – for density ratio  $\gamma = 10$ .

FIGURE 7. Profiles of vorticity-to-strain ratio for density ratio  $\gamma = 2$ . Solid:  $x/d = 0.25$ ; dashed:  $x/d = 0.50$ ; dashdot:  $x/d = 0.75$ ; dotted:  $x/d = 1.0$ .

FIGURE 8. Profiles of vorticity-to-strain ratio for density ratio  $\gamma = 10$ . Solid:  $x/d = 0.25$ ; dashed:  $x/d = 0.50$ ; dashdot:  $x/d = 0.75$ ; dotted:  $x/d = 1.0$ .

FIGURE 9. Normalised difference between the local compressional direction and the equilibrium orientation of the gradient of a passive scalar for density ratio  $\gamma = 6$ .

FIGURE 10. Theoretical growth rate of the norm of a passive scalar gradient normalised by local strain; density ratio  $\gamma = 6$ .

FIGURE 11. Theoretical growth rate of the norm of a passive scalar gradient normalised by the imposed strain; density ratio  $\gamma = 6$ .

FIGURE 12. Trajectories starting from  $x/d = 1$  and  $y/d = 1, 2, 5$  and  $10$ ; density ratio  $\gamma = 6$ .

FIGURE 13. Evolution of strain persistence parameter along trajectories starting from  $x/d = 1$  and  $y/d = 1, 2, 5$  and  $10$ ; density ratio  $\gamma = 6$ .

FIGURE 14. Evolution of equilibrium orientation along trajectories starting from  $x/d = 1$  and  $y/d = 1, 2, 5$  and  $10$ ; density ratio  $\gamma = 6$ .

FIGURE 15. Departure of scalar gradient orientation to equilibrium orientation along trajectories starting from  $x/d = 1$  and  $y/d = 1, 2, 5$  and  $10$ ; density ratio  $\gamma = 6$ .

FIGURE 16. Evolution of the actual growth rate of scalar gradient norm normalised by the imposed strain along trajectories starting from  $x/d = 1$  and  $y/d = 1, 2, 5$  and  $10$ ; density ratio  $\gamma = 6$ .

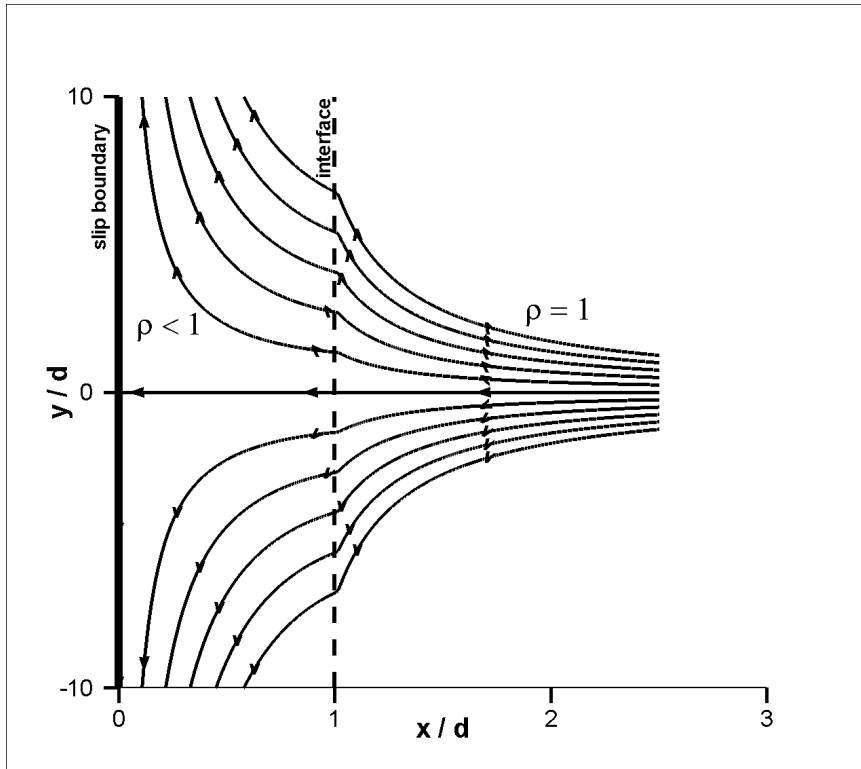


Fig. 1. Stagnation-point flow altered by the density step. Streamlines are plotted for density ratio  $\gamma = 6$ .

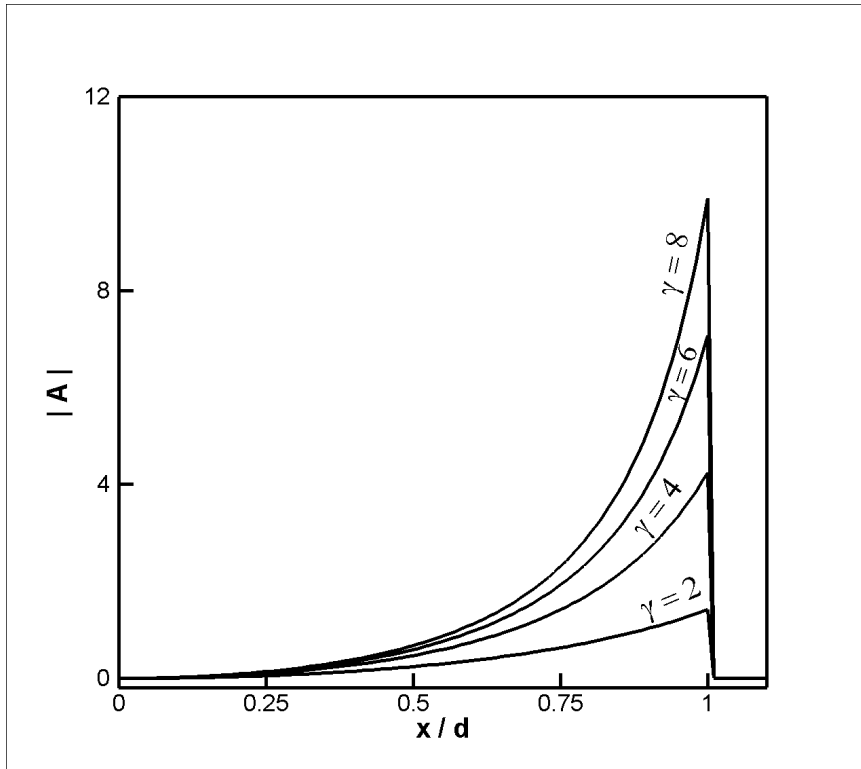


Fig. 2. Effect of density ratio on the norm of the anisotropy tensor of pressure Hessian.

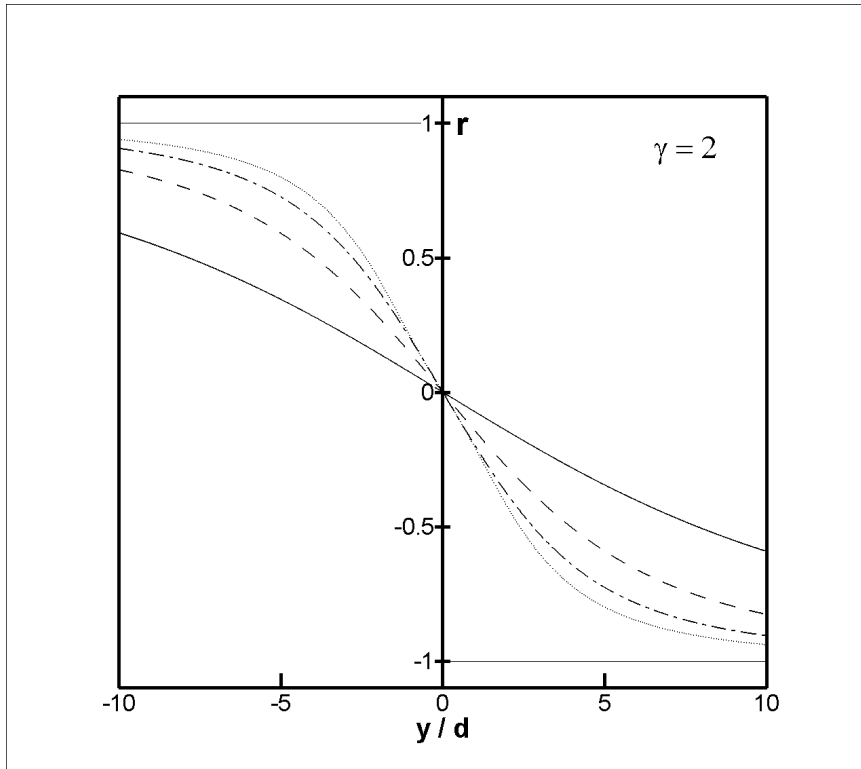


Fig. 3. Profiles of strain persistence parameter for density ratio  $\gamma = 2$ . Solid:  $x/d = 0.25$ ; dashed:  $x/d = 0.50$ ; dashdot:  $x/d = 0.75$ ; dotted:  $x/d = 1.0$ .

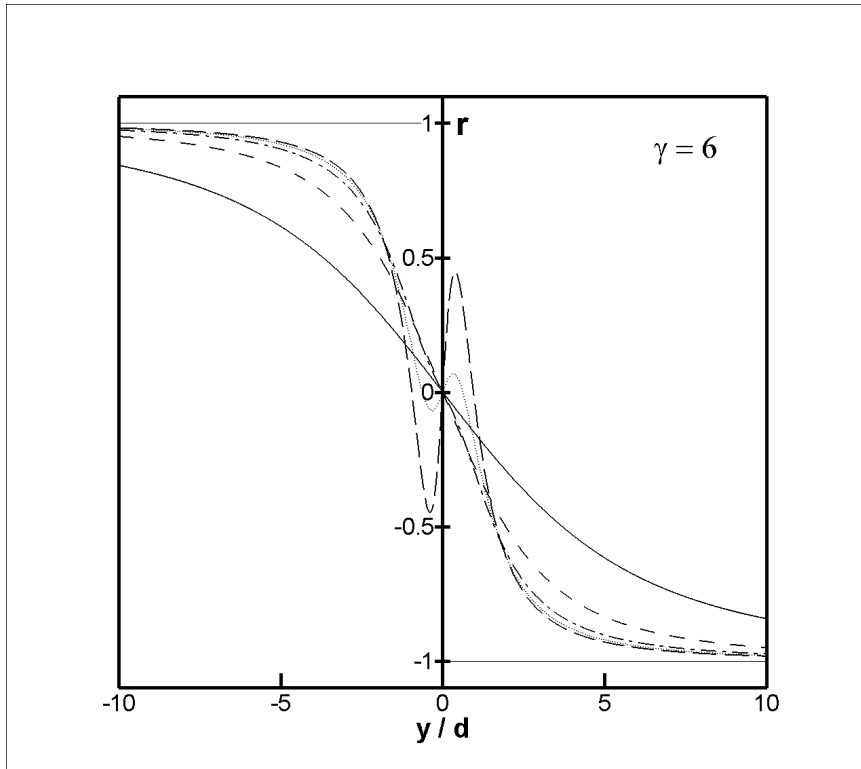


Fig. 4. Profiles of strain persistence parameter for density ratio  $\gamma = 6$ . Solid:  $x/d = 0.25$ ; dashed:  $x/d = 0.50$ ; dashdot:  $x/d = 0.75$ ; dotted:  $x/d = 0.90$ ; longdash:  $x/d = 1.0$ .

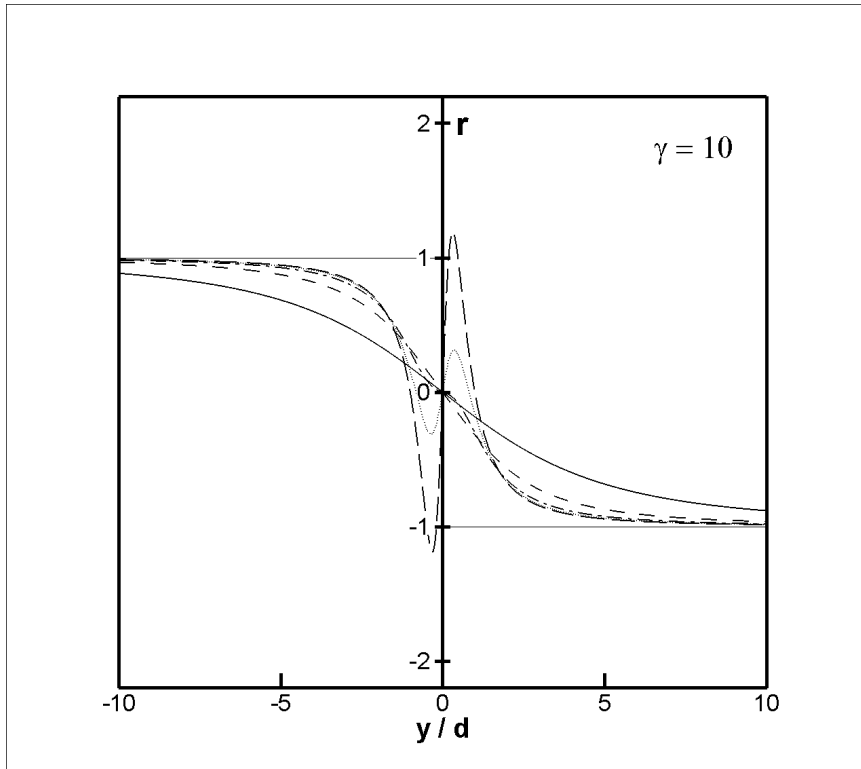


Fig. 5. Profiles of strain persistence parameter for density ratio  $\gamma = 10$ . Solid:  $x/d = 0.25$ ; dashed:  $x/d = 0.50$ ; dashdot:  $x/d = 0.75$ ; dotted:  $x/d = 0.90$ ; longdash:  $x/d = 1.0$ .

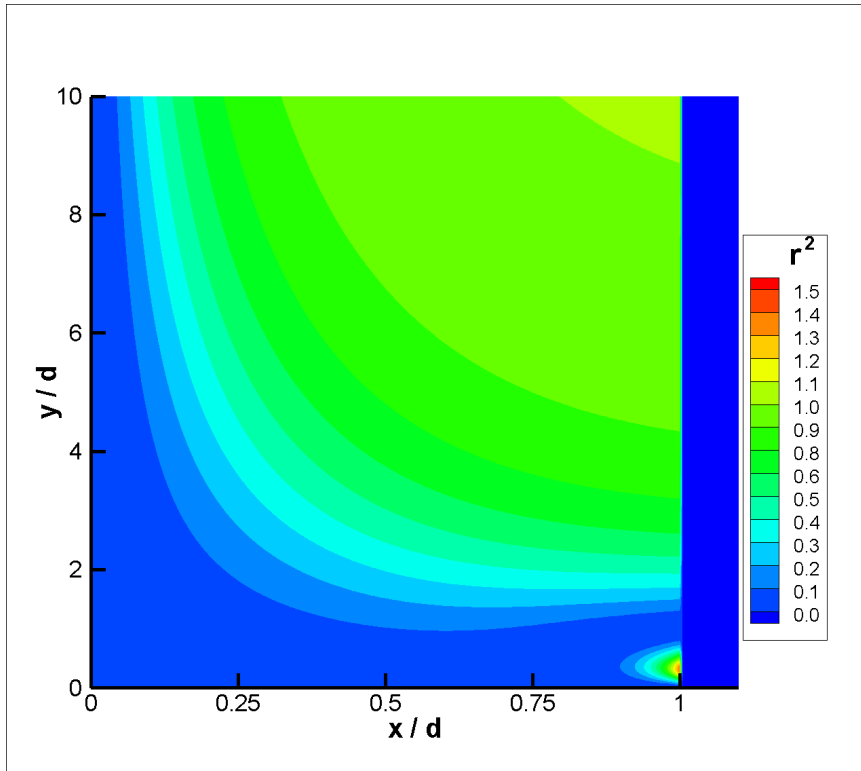


Fig. 6. Field of strain persistence parameter – squared – for density ratio  $\gamma = 10$ .

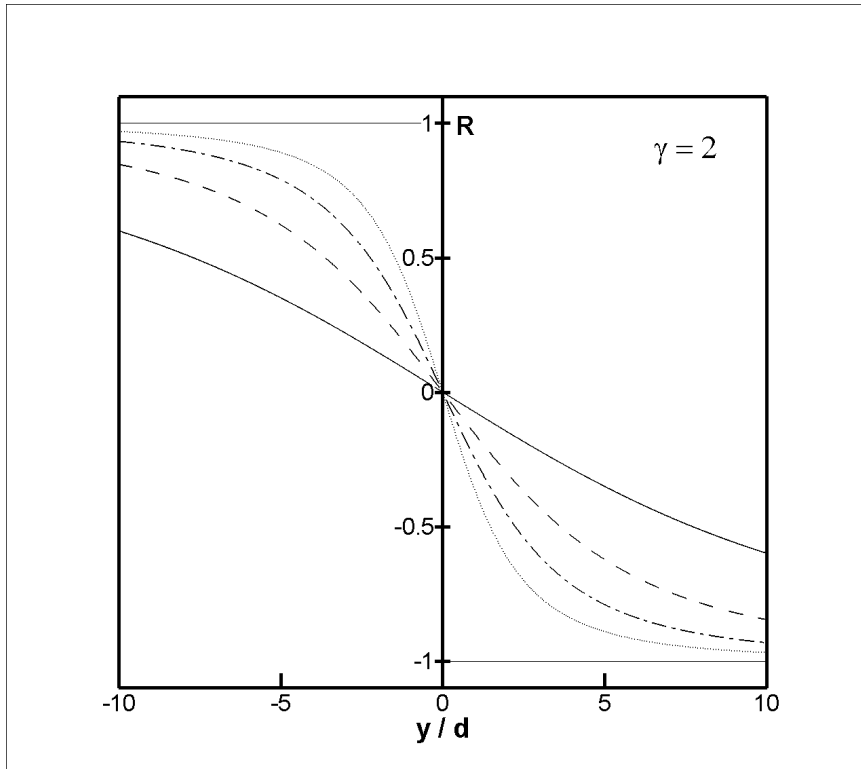


Fig. 7. Profiles of vorticity-to-strain ratio for density ratio  $\gamma = 2$ . Solid:  $x/d = 0.25$ ; dashed:  $x/d = 0.50$ ; dashdot:  $x/d = 0.75$ ; dotted:  $x/d = 1.0$ .

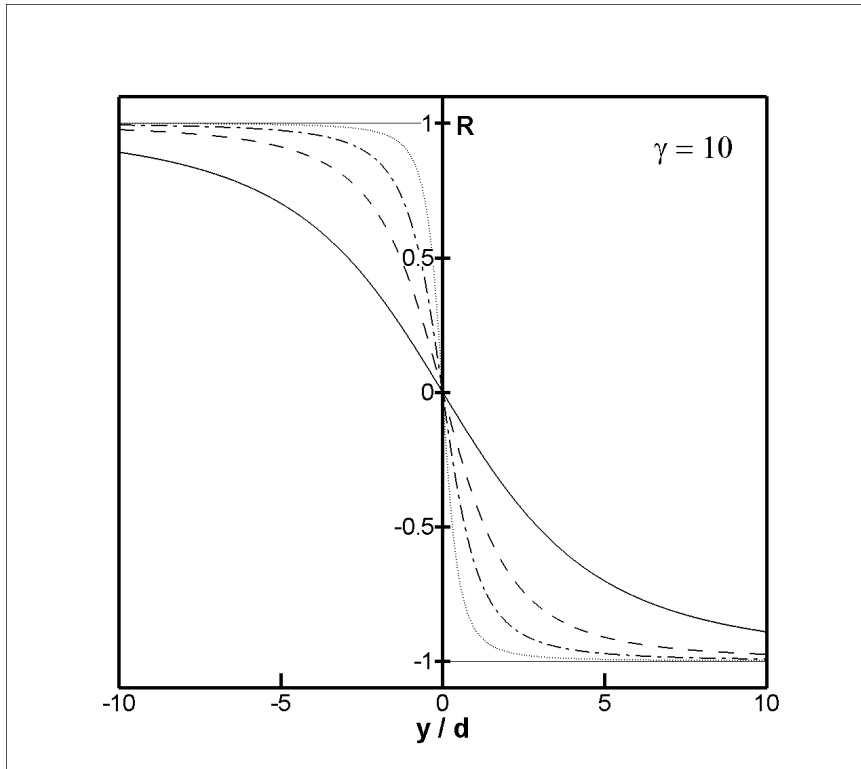


Fig. 8. Profiles of vorticity-to-strain ratio for density ratio  $\gamma = 10$ . Solid:  $x/d = 0.25$ ; dashed:  $x/d = 0.50$ ; dashdot:  $x/d = 0.75$ ; dotted:  $x/d = 1.0$ .

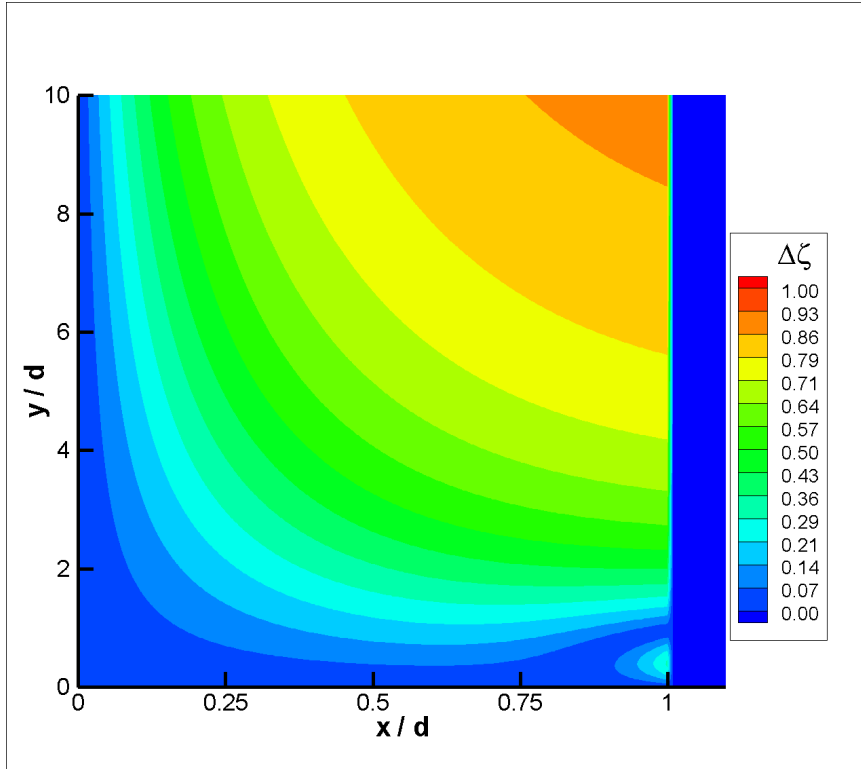


Fig. 9. Normalised difference between the local compressional direction and the equilibrium orientation of the gradient of a passive scalar for density ratio  $\gamma = 6$ .

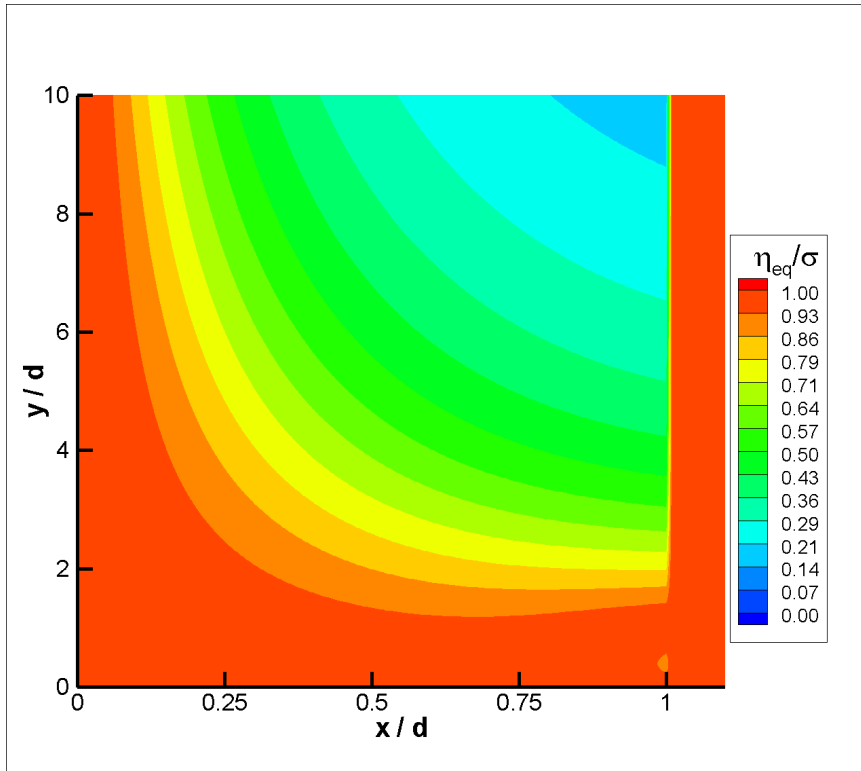


Fig. 10. Theoretical growth rate of the norm of a passive scalar gradient normalised by local strain; density ratio  $\gamma = 6$ .

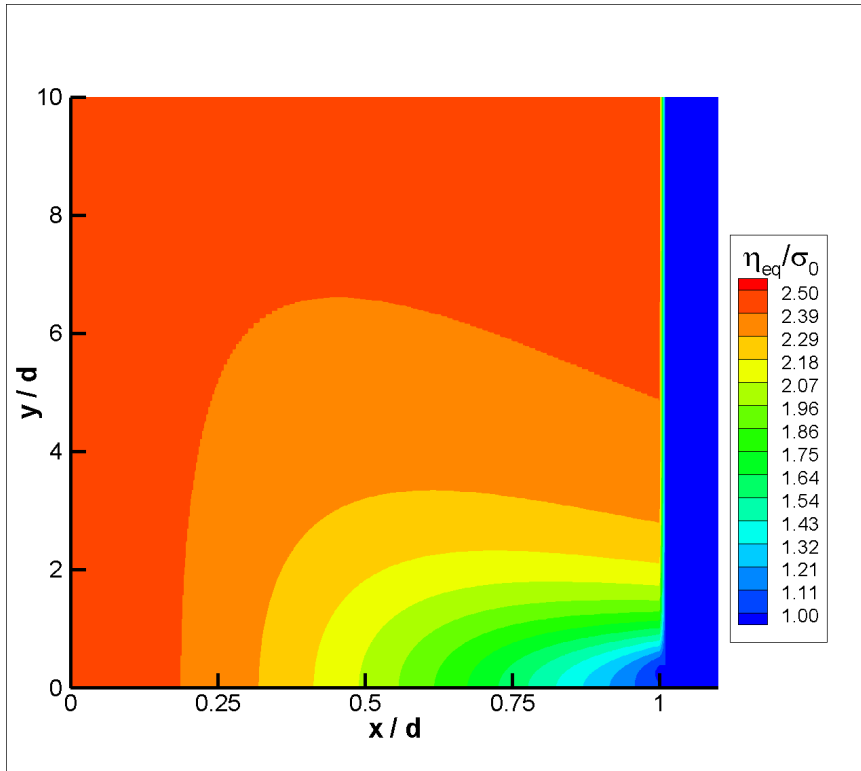


Fig. 11. Theoretical growth rate of the norm of a passive scalar gradient normalised by the imposed strain; density ratio  $\gamma = 6$ .

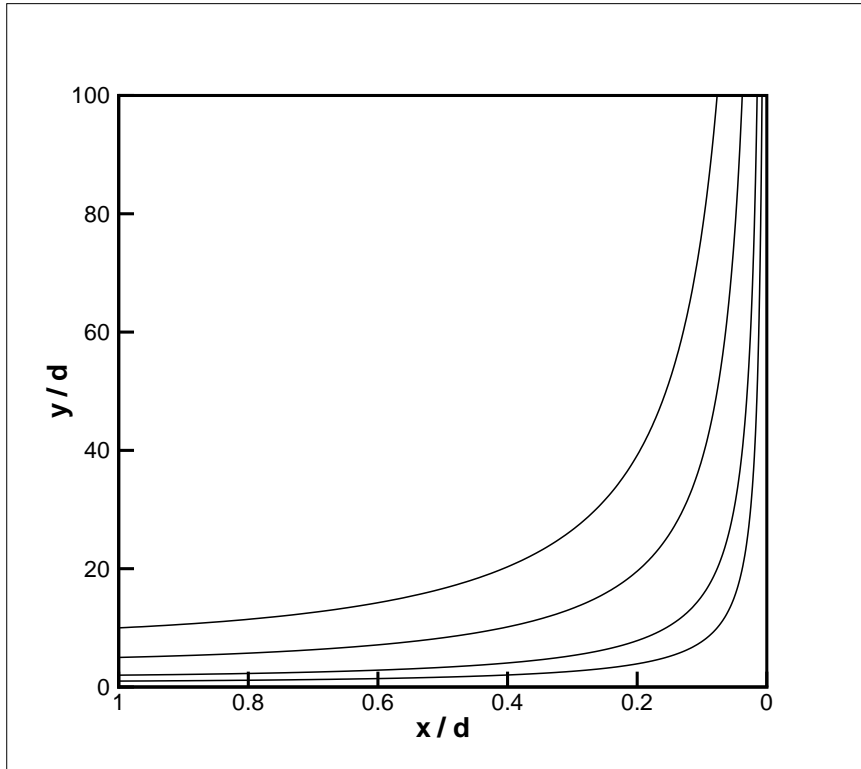


Fig. 12. Trajectories starting from  $x/d = 1$  and  $y/d = 1, 2, 5$  and  $10$ ; density ratio  $\gamma = 6$ .

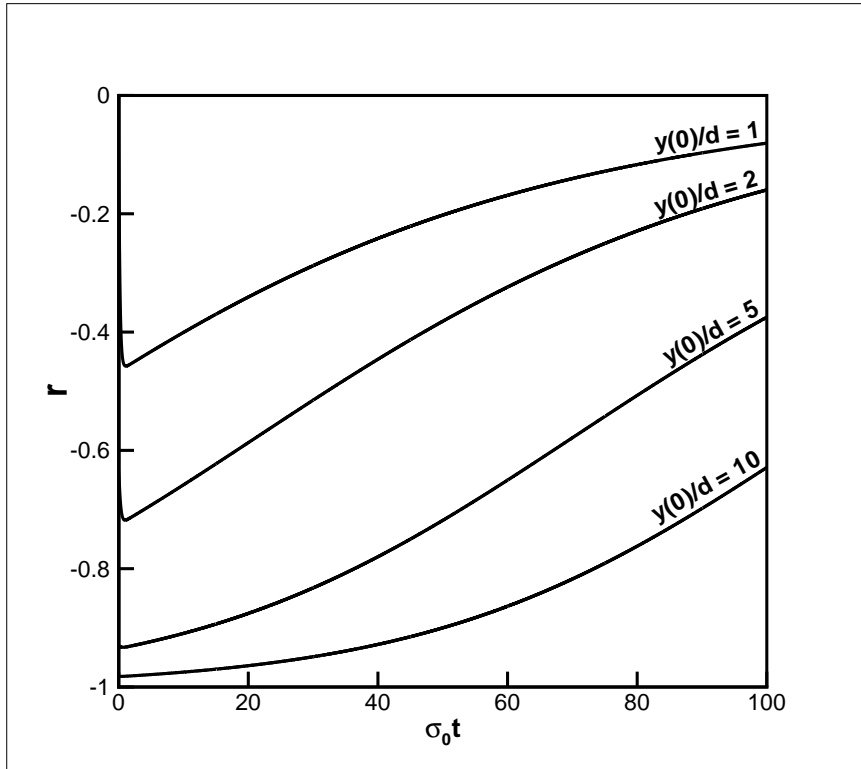


Fig. 13. Evolution of strain persistence parameter along trajectories starting from  $x/d = 1$  and  $y/d = 1, 2, 5$  and  $10$ ; density ratio  $\gamma = 6$ .

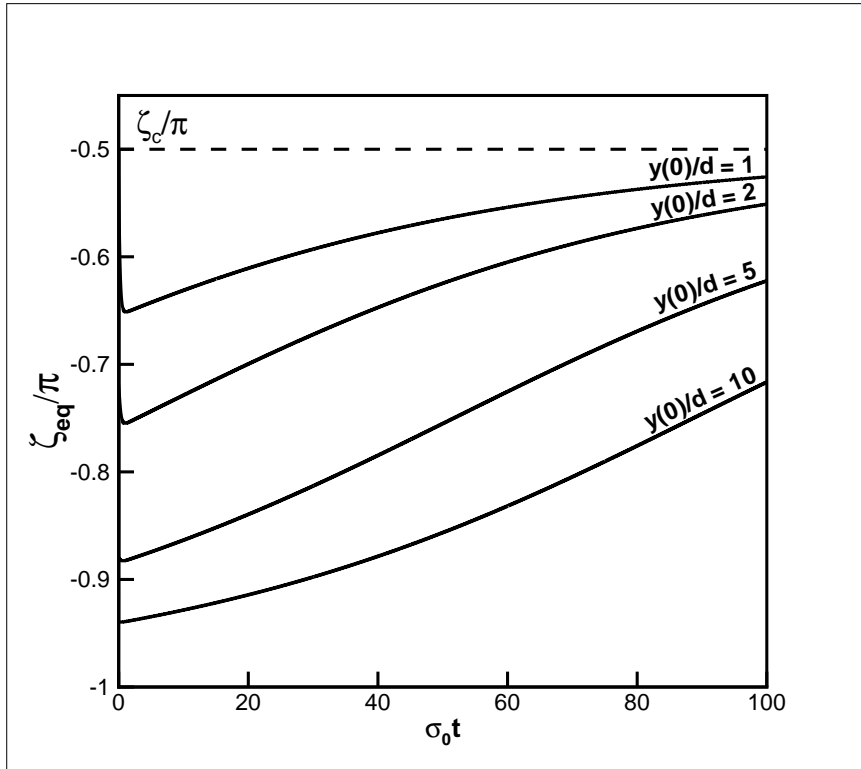


Fig. 14. Evolution of equilibrium orientation along trajectories starting from  $x/d = 1$  and  $y/d = 1, 2, 5$  and  $10$ ; density ratio  $\gamma = 6$ .

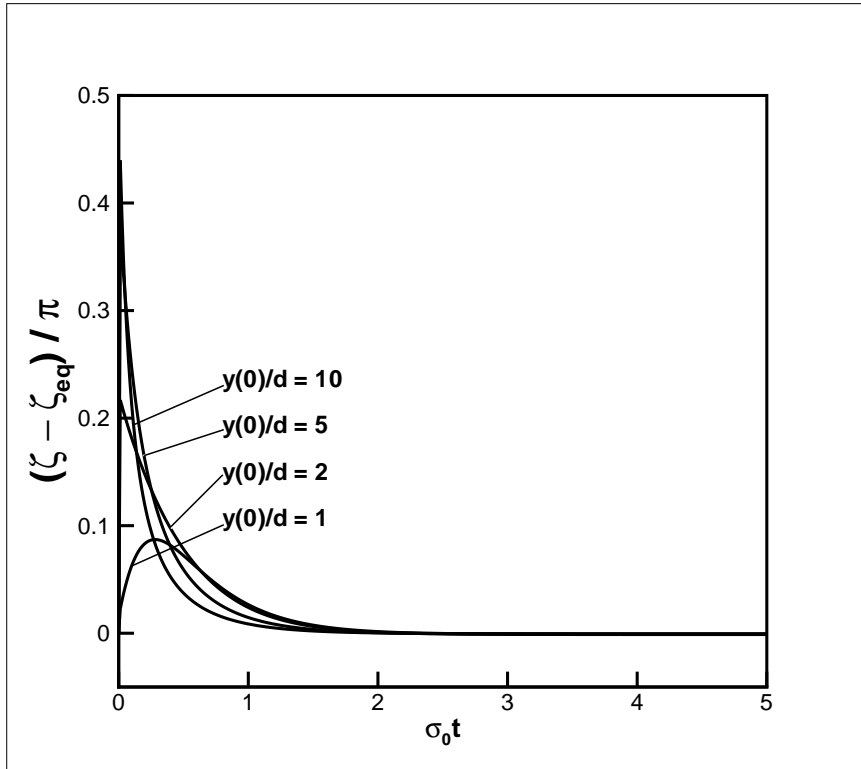


Fig. 15. Departure of scalar gradient orientation to equilibrium orientation along trajectories starting from  $x/d = 1$  and  $y/d = 1, 2, 5$  and  $10$ ; density ratio  $\gamma = 6$ .

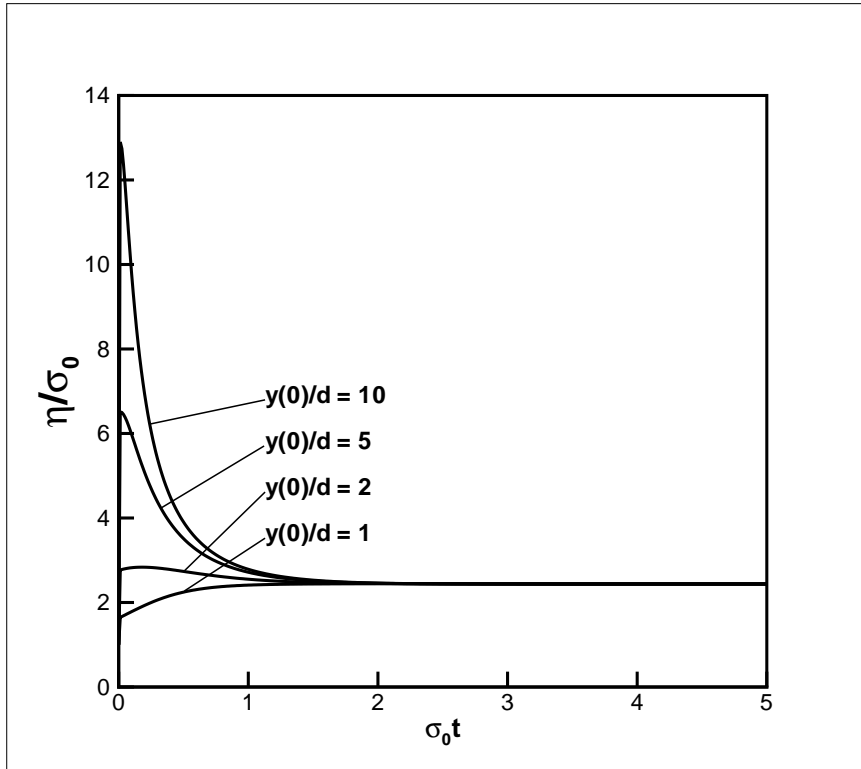


Fig. 16. Evolution of the actual growth rate of scalar gradient norm normalised by the imposed strain along trajectories starting from  $x/d = 1$  and  $y/d = 1, 2, 5$  and 10; density ratio  $\gamma = 6$ .